Chemical Science

ROYAL SOCIETY OF CHEMISTRY

EDGE ARTICLE

View Article Online
View Journal | View Issue

Check for updates

Cite this: *Chem. Sci.*, 2020, **11**, 1316

All publication charges for this article have been paid for by the Royal Society of Chemistry

Synthetic studies of cystobactamids as antibiotics and bacterial imaging carriers lead to compounds with high *in vivo* efficacy†

Giambattista Testolin,[a] Katarina Cirnski,[bc] Katharina Rox,[ab] Hans Prochnow,[a] Verena Fetz,[a] Charlotte Grandclaudon,[ab] Tim Mollner,[a] Alain Baiyoumy,[a] Antje Ritter,[a] Christian Leitner,[ab] Jana Krull,[a] Joop van den Heuvel,[d] Aurelie Vassort,[e] Sylvie Sordello,[f] Mostafa M. Hamed,[c] Walid A. M. Elgaher,[c] Jennifer Herrmann,[bc] Rolf W. Hartmann,[c] Rolf Müller[bc] and Mark Brönstrup *[abg]

Received 20th September 2019
Accepted 4th December 2019

DOI: 10.1039/c9sc04769g

rsc.li/chemical-science

There is an alarming scarcity of novel chemical matter with bioactivity against multidrug-resistant Gram-negative bacterial pathogens. Cystobactamids, recently discovered natural products from myxobacteria, are an exception to this trend. Their unusual chemical structure, composed of oligomeric *para*-aminobenzoic acid moieties, is associated with a high antibiotic activity through the inhibition of gyrase. In this study, structural determinants of cystobactamid's antibacterial potency were defined at five positions, which were varied using three different synthetic routes to the cystobactamid scaffold. The potency against *Acinetobacter baumannii* could be increased ten-fold to an MIC (minimum inhibitory concentration) of 0.06 μg mL^{-1}, and the previously identified spectrum gap of *Klebsiella pneumoniae* could be closed compared to the natural products (MIC of 0.5 μg mL^{-1}). Proteolytic degradation of cystobactamids by the resistance factor AlbD was prevented by an amide-triazole replacement. Conjugation of cystobactamid's N-terminal tetrapeptide to a Bodipy moiety induced the selective localization of the fluorophore for bacterial imaging purposes. Finally, a first *in vivo* proof of concept was obtained in an *E. coli* infection mouse model, where derivative **22** led to the reduction of bacterial loads (cfu, colony-forming units) in muscle, lung and kidneys by five orders of magnitude compared to vehicle-treated mice. These findings qualify cystobactamids as highly promising lead structures against infections caused by Gram-positive and Gram-negative bacterial pathogens.

Introduction

The public health threat posed by bacterial infections has increased to an alarming extent, because bacterial resistance against common antibiotics has risen over the last two decades while, at the same time, an innovation gap in antibiotic discovery led to a shriveled pipeline of novel drugs.[1] This is particularly true for Gram-negative pathogens: since infections with carbapenem-resistant Enterobacteriaceae are associated with mortality rates of 40–50%, these species as well as drug-resistant *Acinetobacter baumannii* and *Pseudomonas aeruginosa* have been classified as 'critical' by the WHO.[2] The main scientific problem that hampers the discovery of novel antibiotics against Gram-negative species concerns the lack of knowledge on how to design molecules that can achieve sufficient intracellular concentrations by overcoming the highly effective penetration barriers imposed by the inner and outer membranes on the one hand, and by avoiding efflux-mediated export on the other hand.[3,4] Recent progress was achieved by establishing structural guidelines for synthetic small molecules,[5] or by antibiotic conjugation to actively transported moieties (the 'Trojan Horse' principle).[6] However, studying natural products arguably remains the most fruitful strategy to discover novel antibiotic lead structures against Gram-negative bacteria.[1,7] This is exemplified by the recently discovered cystobactamids, myxobacterial natural products that exhibit potent, broad-spectrum antibacterial properties through the inhibition of bacterial gyrase A.[8] Cystobactamids, their

---

[a] *Department of Chemical Biology, Helmholtz Centre for Infection Research, Inhoffenstrasse 7, 38124 Braunschweig, Germany. E-mail: mark.broenstrup@helmholtz-hzi.de*

[b] *German Center for Infection Research (DZIF), Site Hannover-Braunschweig, Germany*

[c] *Helmholtz Institute for Pharmaceutical Research Saarland, Universitätscampus E8.1, 66123 Saarbrücken, Germany*

[d] *Group Recombinant Protein Expression, Helmholtz Centre for Infection Research, Inhoffenstrasse 7, 38124 Braunschweig, Germany*

[e] *Evotec ID, 1541 Avenue Marcel Merieux, 69289 Marcy l'Etoile, France*

[f] *Evotec ID, Alderley Park, Cheshire SK10 4TG, UK*

[g] *Center of Biomolecular Drug Research (BMWZ), Leibniz Universität, 30167 Hannover, Germany*

† Electronic supplementary information (ESI) available. See DOI: 10.1039/c9sc04769g

derivatives coralmycin[9] and the closely related albicidin[10] are featured by an unusual aromatic oligopeptide structure, composed of five *para*-aminobenzoic acid (PABA)-derived moieties and a central aliphatic amino acid (Scheme 1). An in-depth isolation study from *Myxococcus* sp. resulted in the discovery of derivative 861-2 as the most potent cystobactamid analog.[11] Soon after their first isolation, total syntheses of albicidin (**1**) and the cystobactamids 861-2 (**2**) and 919-2 (**3**) were reported,[11–15] all highlighting the hidden challenges behind the chemistry of these natural products, such as low reactivity in aromatic amine couplings combined to solubility problems. First variations of the albicidin structure at various positions led to mostly equal antibacterial activity compared to the natural product.[16–19]

In this paper, we report the establishment of three different synthetic routes for a systematic study of cystobactamid's structure–activity relationships (SAR), in order to optimize the activity profile across a larger panel of bacterial pathogens. We obtained compounds with significantly improved antibacterial activity, and a rescaffolding of the C-ring led to the circumvention of AlbD-mediated resistance, an endopeptidase that site-specifically cleaves albicidin in two inactive fragments. Furthermore, a proof of principle that the cystobactamid scaffold can be used as a targeting moiety for bacterial imaging is provided. Finally, the pharmacokinetic properties as well as a first *in vivo* proof of concept of derivative **22** are presented.

Results

Cystobactamids do not obey the guidelines for physicochemical properties that are important for activity against Gram-negative bacteria: according to O'Shea and Moser, a low molecular weight (cutoff *ca.* 600 Da) and high polarity are important features of Gram-negative antibiotics to facilitate transport through porin channels.[20] In addition, the so-called "eNTRy" rules proposed by Richter *et al.* state that accumulation in Gram-negative bacteria is more likely to occur if a molecule possesses basic nitrogens (primary amines being optimal), low globularity and high rigidity.[5] In contrast, cystobactamids have no basic nitrogen, their molecular weight (>850 Da) is far beyond the cutoff, they are highly nonpolar (clog $P = 4.19$), and 15 (principally) rotatable bonds limit their rigidity (ESI Section 2†). Because the potent activity of cystobactamids against Gram-negative pathogens is achieved with atypical physicochemical properties, we did not apply such parameters as filters for compound design. In the absence of structural information on the binding to gyrase and on uptake determinants, the synthesis of novel compounds was driven by their antibacterial activity and their ability to inhibit gyrase.

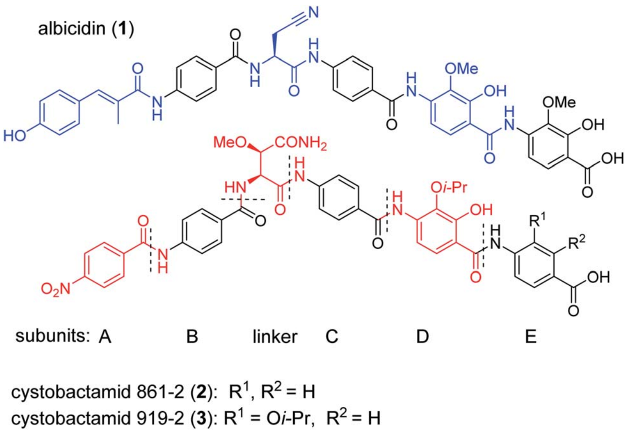

Scheme 1 Chemical structures of albicidin and cystobactamids 861-2 and 919-2. Characteristic structural features of the classes are highlighted in blue for albicidin and in red for cytobactamids.

In order to understand the minimal structural requirement for high antibiotic activity, a simplification of the cystobactamid structure was targeted, starting with the most potent analog **2**. We first decided to investigate the relevance of the methoxy group in the central linker region, as the high activity of albicidin suggested that a substituent at position C-3 of the aliphatic amino acid may not be mandatory. Therefore, the desmethoxy analog **4** was synthesized following the retrosynthetic approach that we recently reported[11] for the total synthesis of **2** (Scheme 2), with the main difference that the central fragment **6** bears L-Asn instead of the (2*S*,3*R*)-β-methoxy-Asn moiety of **2**.

In brief, Fmoc-Asn(Trt)-OH and methyl-*p*-aminobenzoate were coupled efficiently by means of $POCl_3$ at 0 °C. Keeping the temperature low was important in order to avoid racemization of the aliphatic amino acid (Scheme 3).[21] After deprotection of the Fmoc group, the second PABA unit was installed using HBTU and *para*-nitrobenzoic acid (PNBA) to give **94** in 78% yield. Because the ester hydrolysis under standard hydrolytic conditions (LiOH, water/THF) led to complete racemization, the carboxylic acid **6** was obtained using an excess of LiI in ethyl acetate under refluxing conditions.[22]

Fragment **7**, synthesized as reported previously,[11] was coupled to **6** using $POCl_3$ to obtain the pentapeptide **11**. The reduction of the nitro group and the removal of the trityl protecting group afforded **12**. The N-terminal PNBA moiety was activated as an acyl chloride and coupled to **12**. After the removal of the allyl protecting groups and a final purification by preparative reversed phase (RP) HPLC, **4** was obtained as an ammonium salt. A Marfey analysis,[23–25] used to assess the enantiomeric ratio, revealed that less than 5% of racemization occurred during the synthesis (see ESI†). The overall synthesis had 12 steps in the longest linear sequence and an overall yield of 1.9%.

The minimal inhibitory concentrations (MICs) of all compounds were determined against a small panel of three clinically important pathogens comprising *Escherichia coli*, *Pseudomonas aeruginosa* and *Staphylococcus aureus*. For the two former species, mutants with impaired efflux (*E. coli* ΔtolC and *P. aeruginosa* ΔmexAB) were tested in order to assess transport-mediated effects. In addition, a functional gyrase supercoiling assay served to probe the target-specific activity of the cystobactamids. Compound **4** showed high antibacterial activities that were comparable to those of **2**, with the notable exception of a strongly decreased activity against *P. aeruginosa* (Table 1). The overall profile confirmed the assumption of the β-methoxy group in the central amino acid linker is not essential. Because

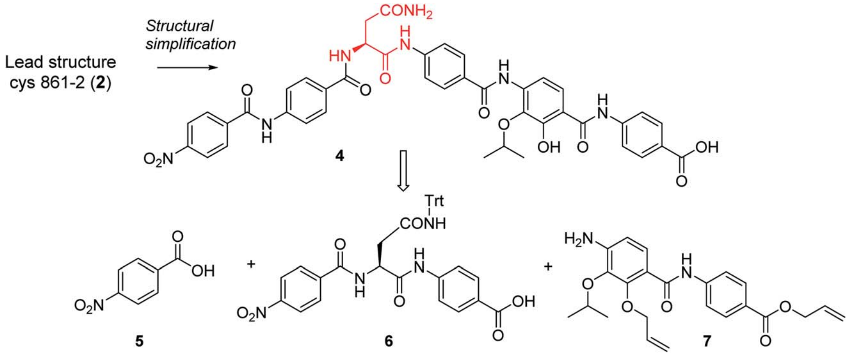

Scheme 2 Retrosynthetic disconnection of **4**.

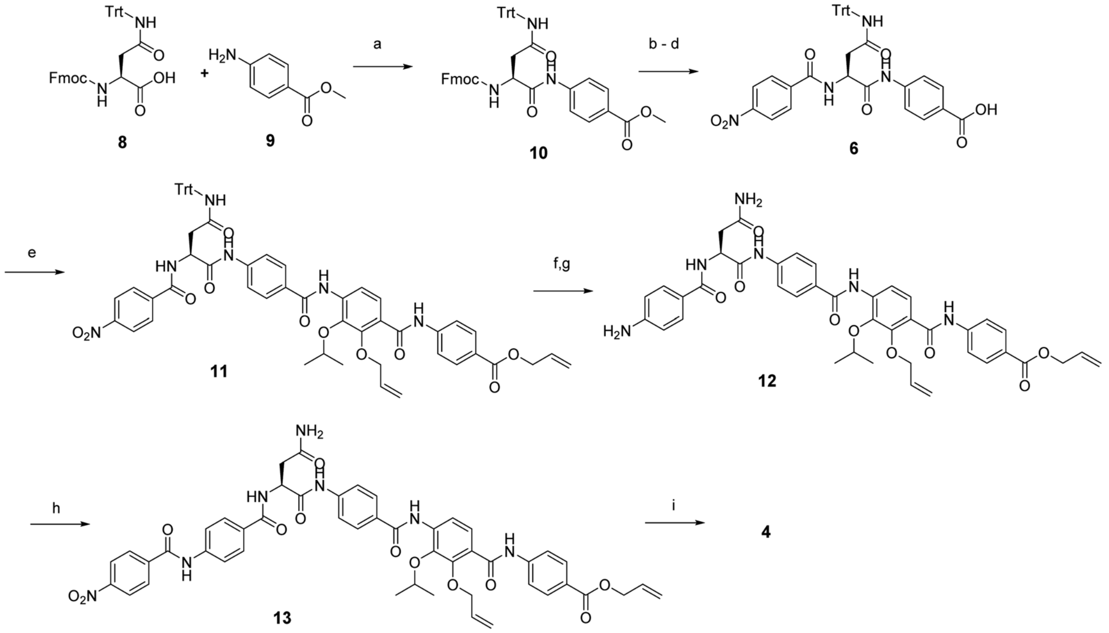

Scheme 3 Reagent and conditions: (a) $POCl_3$, TEA, DCM, 0 °C, 2 h (96%); (b) 20% Et_2NH in CH_3CN, rt, 30 min; (c) HBTU, DiPEA, CH_3CN, rt, 3 h (78% 2 steps); (d) LiI, EtOAc, 90 °C, 5 d (86%); (e) amine **7**, $POCl_3$, DiPEA, THF/DCM, rt, 6 h (54%); (f) Zn dust, 10% AcOH, THF/EtOH, rt, 5 h, (g) TFA, Tips, DCM (94% 2 steps); (h) 4-nitrobenzoic acid, BTC, collidine, DiPEA, THF, rt, 4 h (80%); (i) $Pd(PPh_3)_4$; $PhSiH_3$, THF, rt, overnight (21%).

4 was slightly more potent than **2** in a target-based gyrase supercoiling assay (IC_{50} values of 0.11 μM *vs.* 0.22 μM), the additional methoxy moiety of **2** seems to be beneficial for intracellular compound accumulation in *P. aeruginosa* WT.

As the synthesis of **4** was more amenable to scale up compared to that of **2**, a series of cystobactamid analogs bearing L-asparagine as a central element was designed that carry alterations in the N-terminal (ring A) and C-terminal (rings D–E) regions of the molecule.

A-ring variations

For A-ring variations, the advanced intermediate **12** was coupled to different carboxylic acids that varied in the nature, number

Table 1 Antibacterial activity of **2** and **4**, given as minimal inhibitory concentrations (MICs) in μg mL^{-1}, and inhibitory activity against DNA gyrase in μM

	MIC [μg mL^{-1}]					
Compound	*E. coli* ΔtolC[a]	*E. coli* WT[b]	*P. aeruginosa* ΔmexAB[a]	*P. aeruginosa* WT[c]	*S. aureus*[d]	*E. coli* gyrase IC_{50} [μM]
2	0.125	0.125	0.5	2	0.5	0.22
4	0.125	1	1	>64	1	0.11

[a] Strain provided by collaborators, see ESI. [b] DSM-1116. [c] PA14. [d] ATCC29213.

Table 2 Antibacterial activity of cystobactamid A-ring analogs, given as minimal inhibitory concentrations (MICs) in μg mL^{-1}, and inhibitory activity against DNA gyrase in μM[e]

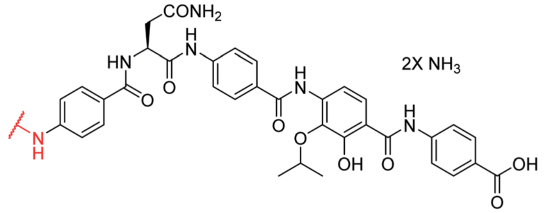

	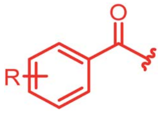			MIC [μg mL^{-1}]					
	R								
Compound	*o*	*m*	*p*	*E. coli* ΔtolC[a]	*E. coli* WT[b]	*P. ae.* ΔmexAB[a]	*P. ae.* WT[c]	*S. aureus*[d]	*E. coli* gyrase IC$_{50}$ [μM]
Reference 4	**H**	**H**	**NO_2**	**0.125**	**1**	**1**	**>64**	**1**	**0.11**
14	H	H	NHAc	0.06	16	>64	>64	64	nd
15	H	H	H	0.5	>64	2	>64	>64	4.0
16	H	H	F	0.5	0.5	2	>64	2	nd
17	H	H	NH_2	32	2	4	>64	>64	26.8
18	H	NO_2	H	0.25	>64	0.5	>64	>64	2.2
19	H	NH_2	H	2	32	4	>64	>64	nd
20	NO_2	H	H	2	8	16	>64	>64	nd
21	H	H	$NHCONH_2$	≤0.03	0.5	4	>64	64	8.7
22	H	H	CN	0.06	0.5	0.25	2	0.25	0.08
23	H	H	CF_3	≤0.03	0.5	64	>64	16–32	nd
24	H	H	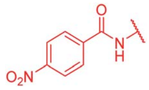	>64	0.5	>64	>64	>64	2.5
25	OH	i-PrO	NO_2	>64	>64	>64	>64	>64	>50
26	OH	i-PrO	NH_2	0.01	2	2–4	32	>64	50
27	H	H	SO_2CH_3	≤0.03	2	4	>64	>64	nd
28	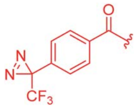			8	16	>64	>64	>64	16
29	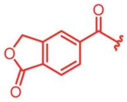			≤0.03	≤0.03	1	>64	1	1.4
30	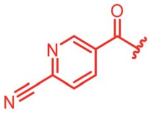			≤0.03	≤0.03	1	>64	64	0.5
31	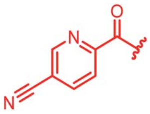			≤0.03	≤0.03	0.25	0.5	≤0.03	0.9
32	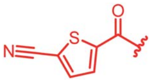			≤0.03	≤0.03	0.25	0.5	0.25	0.5
33	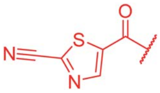			≤0.03	0.06	1	>64	4	nd

Table 2 (*Contd.*)

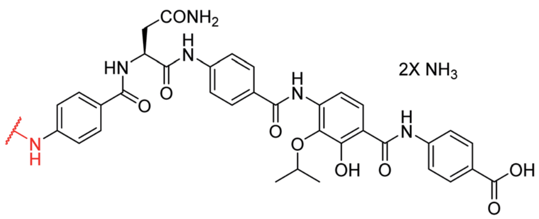

				MIC [μg mL^{-1}]					
	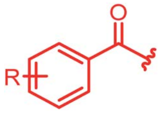								
	R								
Compound	*o*	*m*	*p*	*E. coli* ΔtolC[a]	*E. coli* WT[b]	*P. ae.* ΔmexAB[a]	*P. ae.* WT[c]	*S. aureus*[d]	*E. coli* gyrase IC$_{50}$ [μM]
34		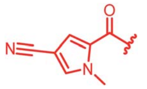		≤0.03	≤0.03	0.5	>64	64	0.7
35		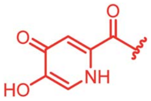		>64	>64	>64	>64	>64	3.6
36		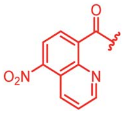		0.5	0.25	>64	>64	>64	0.3

[a] Strain provided by collaborators, see ESI. [b] DSM-1116. [c] PA14. [d] ATCC29213. [e] nd = not determined, *P. ae.* = *P. aeruginosa*.

and position of substituents (ESI Scheme S1†). The acids were activated as acyl chlorides by means of BTC and collidine[12] or oxalyl chloride. Alternatively, when the substituents required a milder activation strategy, a combination of EDC and HOAt was chosen. Most derivatives were purified by preparative RP-HPLC with a water/acetonitrile gradient using 10 mM NH_4HCO_3 as a modifier and obtained as ammonium salts.

The antibacterial properties of all analogs were determined subsequently (Table 2). The electronic properties and the position of the N-terminal substituent turned out to be essential, as the replacement of the nitro group by a hydrogen atom in **15** was associated with a drop of activity against *E. coli* from 1 μg mL^{-1} to >64 μg mL^{-1}. Also its shift from the *para*-to *meta*- and *ortho*-positions led to MICs of >64 μg mL^{-1} and 8 μg mL^{-1}, respectively. Likewise, reduced analogs bearing an amino group (**17**) or an *N*-acetylamino group (**14**) had lower activities of 2 μg mL^{-1} and 16 μg mL^{-1}, respectively. An ureido substitution as in **21** resulted in equipotent compounds against *E. coli*, but reduced activity against *S. aureus* or *P. aeruginosa*. Also the installation of a photoactivatable trifluoromethyl-diazirine moiety at the *para*-position led to pronounced drops in gyrase inhibition and antibacterial activity, suggesting that **28** is not ideally suited for the mapping of the gyrase binding site in cross-linking experiments.

As cystobactamids are PABA oligomers, we wondered whether their elongation to a heptapeptide by the addition of another PNBA moiety to the N-terminus would further enhance potency. However, **24** showed a 20-fold reduced inhibitory activity in the gyrase assay and displayed worse antibacterial activity compared to **4**. We then copied the substitution pattern of the oxidized D-ring of cystobactamids to the N-terminus. The obtained compound **25** neither showed acceptable gyrase inhibition nor any antibacterial activity. In contrast, the replacement of the nitro group with other electron-withdrawing substituents like trifluoromethyl (**23**) or fluorine (**16**) retained antibiotic activity or even improved them, as observed for a cyano (**22**) or a lactone moiety (**29**). The cyano group was identified as particularly favorable, because **22** also displayed a strongly increased activity against *P. aeruginosa* (2 μg mL^{-1} *vs.* >64 μg mL^{-1} for **4**); this substituent was therefore retained in most subsequent analogs. The introduction of a second substituent in *ortho*- or *meta*-position, as in **88–92**, did not lead to improved properties (see Table S1 of the ESI†).

Table 3 Antibacterial activity of cystobactamids with different A–B linkers, given as minimal inhibitory concentrations (MICs) in µg mL^{-1}, and inhibitory activity against DNA gyrase in µM[e]

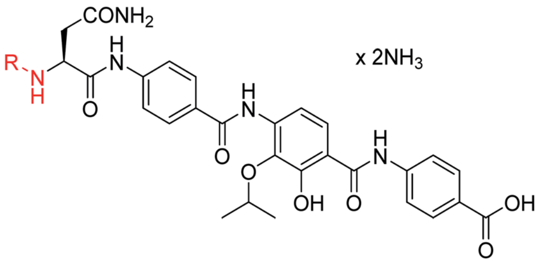

Compound	R	MIC [µg mL^{-1}]					*E. coli* gyrase IC$_{50}$ [µM]
		E. coli ΔtolC[a]	*E. coli* WT[b]	*P. ae.* ΔmexAB[a]	*P. ae.* WT[c]	*S. aureus*[d]	
Reference 22	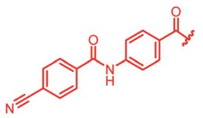	**0.06**	**0.5**	**0.25**	**2**	**0.25**	**0.08**
39	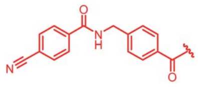	1	>64	>64	>64	>64	nd
40	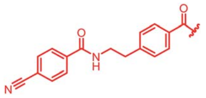	0.125	0.25	4	>64	>64	nd
41	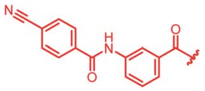	>64	>64	>64	>64	>64	nd
42	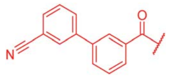	>64	>64	>64	>64	>64	>50
43	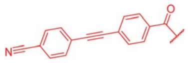	0.06	0.06	0.5	>64	≤0.03	0.5
44	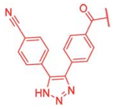	>64	>64	>64	>64	>64	>50
45	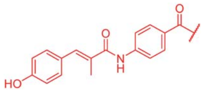	0.06	0.25	0.25	1	0.25	nd
46	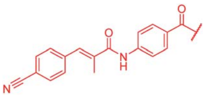	≤0.03	0.125	0.25	1	0.06	0.2
47	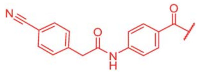	≤0.03	1	>64	>64	>64	16.3
48	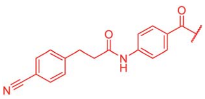	≤0.03	0.125	0.5	>64	>64	1.0
49	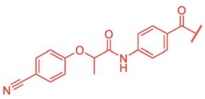	≤0.03	0.06	>64	>64	>64	1.8

Table 3 (*Contd.*)

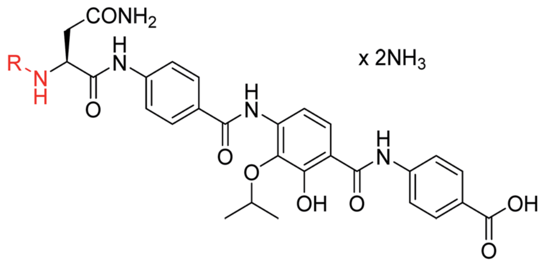

Compound	R	MIC [μg mL^{-1}]					*E. coli* gyrase IC$_{50}$ [μM]
		E. coli ΔtolC[a]	*E. coli* WT[b]	*P. ae.* ΔmexAB[a]	*P. ae.* WT[c]	*S. aureus*[d]	
50	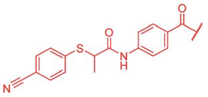	≤0.03	0.25	>64	>64	>64	0.8
51	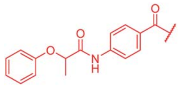	4	>64	>64	>64	>64	nd

[a] Strain provided by collaborators, see ESI. [b] DSM-1116. [c] PA14. [d] ATCC29213. [e] nd = not determined, *P. ae.* = *P. aeruginosa*.

In attempts to replace the phenyl ring, heterocyclic moieties with different electronic properties and ring size were prepared, including the electron-poor pyridines **30** and **31**, the thiophene **32** and the thiazole **33**, and, due to its ability to interact with DNA bases,[26] the electron-rich *N*-methyl pyrrole **34**. A hydroxypyridinone heterocycle with iron-chelating properties was applied (**35**), as this moiety has been successfully attached to β-lactams as a siderophore mimic to enhance their permeation into Gram-negative bacteria through iron uptake pathways.[27,28] Finally, the quinoline **36** should inform whether an extended π-system was favorable for gyrase binding.

The position of the nitrogen in pyridyl analogs mattered, because the 2-carboxyamide-5-cyano-substituted derivative **31** was highly potent against all tested strains, whereas the 3-carboxyamide-6-cyano derivative (**30**) was inactive against *S. aureus* and *P. aeruginosa*. A consistently high antimicrobial activity was also observed for the thiophene **32**, whereas the pyrrole **34** and the quinoline **36** lost activity against *S. aureus* and *P. aeruginosa*. The introduction of an iron-chelating motif (**35**) led to a complete loss of antimicrobial activity and to significantly reduced anti-gyrase activity. After optimizing ring A, we decided to re-introduce the methoxy in the central asparagine, peculiar of the natural cystobactamids, to further assess its influence on the biological activity (ESI†). Remarkably, this molecule showed potent activity against all strains of the small panel of pathogens (analog **93**, Table S1†).

In summary, the A-ring turned out to be a sensitive structural handle for the breadth of the antibacterial spectrum and the potency of cystobactamids. The most important findings are that a hydrogen bond acceptor and small substituents at the *para*-position are essential for a high antibiotic activity, and that the replacement of PABA with heterocyclic moieties is tolerated.

Variations of the linker between A and B rings

A key structural difference between cystobactamids and the closely related albicidin **1** concerns the N-terminus, which is spanned by a *para*-hydroxy-2-methylcinnamoyl moiety in **1**. To assess the impact of this substitution, **45**, a hybrid of the two structures, was synthesized by replacing the PNBA unit of **4** with *para*-hydroxy-2-methylcinnamoyl. Compound **45** indeed possessed high antibiotic activity on all tested strains, including an MIC of 1 μg mL^{-1} against *P. aeruginosa*. As electron-donating substituents in the N-terminal ring of cystobactamids were unfavorable (see above), the *para*-hydroxy group of **45** was replaced by a cyano group to yield **46**, but surprisingly, this change led to an overall unaltered antibacterial potency (Tables 3 and 7).

The fact that the aromatic A and B rings can be connected by a methacrylamide instead of an amide moiety inspired us to vary the length and chemical nature of this region. To access broader diversifications of the N-terminus, a modified synthetic strategy with a late introduction of pre-functionalized A and B rings was adopted (Scheme 4). First, the fragments **38** and **7** were coupled, followed by the cleavage of allyl- and Fmoc-protecting groups. The obtained deprotected tetrapeptide was then coupled to a diaryl unit that comprised rings A and B. The advantages of this approach over the one presented in Scheme 2 are the higher reactivity of the primary, aliphatic amine in the last coupling step and a shortened longest linear sequence (11 steps).

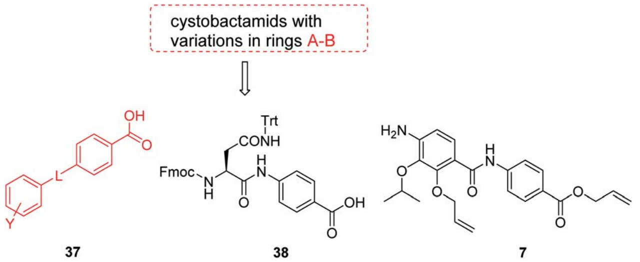

Scheme 4 Retrosynthetic disconnection of cystobactamid with modified A–B rings.

First, the CH═CMe fragment of methacrylamide of **46** was replaced by saturated (CH_2–CH_2 as in **48**), heteroatom-substituted (O–CHMe as in **49**, S–CHMe as in **50**) or truncated linkers (CH_2 as in **47**). In addition, one or two methylene units were introduced between the *para*-cyanobenzamide terminus of **22** and the B-ring to yield **39** and **40**, respectively. The high cellular activity against *E. coli* was retained, but the fact that none of the compounds inhibited *S. aureus* or *P. aeruginosa* demonstrates that the structure–activity relationship (SAR) for a cellular activity is steep and organism-specific at this position.

The impact of the B-ring topology on activity was probed by **41** and **42**, which possess a *meta*-connectivity on ring B; both compounds were completely inactive. In order to investigate whether the amide linking rings A and B in cystobactamid adopts a *cis* or *trans* conformation upon binding to gyrase, **43**, linearized by an alkyne moiety, and the triazole **44**, mimicking a *cis*-conformation, were synthesized. While **43** retained high gyrase inhibition and antibacterial activities, **44** was inactive in both assays. This led us to conclude that (i) a *para*-substitution at the B-ring and a stretched or *trans*-conformation between A and B is required for gyrase binding and (ii) the original amide linker of natural cystobactamids is not required, but can be replaced by a rod-like alkyne connector. However, the original linker between A and B rings had the best overall properties and was therefore retained in subsequent optimizations.

D-ring modifications

Two selected modifications of the D-ring were targeted. An analog of **4**, devoid of the free hydroxy group, was assembled in 10 steps (ESI Schemes S4 and S5†). The analog **52** lost all activity against wild type pathogens, but prevented the growth of efflux-impaired strains, which underlines the crucial importance of the hydroxy group for antibiotic function. In line with this, also the masking of the hydroxy group by an allyl ether as in **13** led to a complete loss of antibacterial activity (Table 4). It is noteworthy that the amide bond between rings D and E is unusually acidic ($pK_a < 8$), as manifested by the comparison of ^1H-NMR data between the ammonium salt with the free acid analog of **4** (ESI Fig. S12†). Both the signals of the amide and the phenolic protons were absent in the spectra of the ammonium salt, which could be attributed to the presence of an anionic, hydrogen-bonded six-membered ring.

Next, the isopropoxy substituent of the D-ring was elongated by a single methylene unit to further increase the bulkiness of this structural feature, yielding **53** (Table 4). This rather subtle structural modification led to an eight-fold decrease of gyrase activity and a complete loss of activity against *E. coli* wild type and the *P. aeruginosa* ΔmexAB mutant. Two derivatives (**54**, **55**) combining the isobutoxy residue and optimized N-terminal ring substitutions could restore the activity against *E. coli* WT, but not against *P. aeruginosa*. On the other hand, a natural cystobactamid with an ethoxy-substitution at the D ring also showed decreased antibacterial activity.[11] Both results underline the importance of the D-ring substitution pattern and imply that the substituent pattern of natural cystobactamids is optimal.

Furthermore, a drastic re-scaffolding was investigated: cystobactamids target subunit A of bacterial DNA gyrase.[8] As this subunit is responsible for interactions with DNA,[29] we hypothesized that it could be beneficial to incorporate a motif into the antibiotic which itself has strong DNA binding properties. Among the high-affinity DNA minor groove recognition elements reported in the literature,[30,31] we selected a minor groove binder developed by Renneberg and Dervan[26] that contains a 4-hydroxybenzimidazole as well as an *N*-methylpyrrole moiety (a Hz/Py pair) and incorporated it into the cystobactamid scaffold. In an attempt to maintain the overall architecture of cystobactamids, the Hz/Py pair replaced the C and D rings of cystobactamids in **56** (Scheme 5). The synthesis of this compound was impaired by solubility and reactivity limitations, but succeeded with an approach that relied on the disconnection in the two fragments **58** and **59**. The fragments were coupled following the activation of the carboxylic acid to an acyl fluoride to avoid potential side reactions of asparagine, such as intramolecular cyclization.[32–34] In sum, **56** was assembled in 11 steps (longest linear sequence) in a total yield of 8.2% (Schemes S6 and S7†).

Compound **56** inhibited bacterial gyrase with an IC_{50} of 10.9 μM, which represents an approximately 100-fold decrease in activity compared to **22**. In consequence, **56** did not exert antibacterial activities at concentrations up to 64 $\mu g\ mL^{-1}$ (ESI Table S2†). This result reflects that the re-scaffolding represents a high risk approach in the absence of information on cystobactamid-target interactions, and it also underlines the high importance of obtaining structural data on cystobactamid binding to inform a rational analog design.

A potential Achilles heel of oligo-PABA antibiotics was recently characterized by Süssmuth and coworkers: the endopeptidase AlbD, expressed by the Gram-negative Enterobacterium *Pantoea dispersa*, was shown to cleave the amide bond connecting C and D rings in **1** as well as in a tripeptide carrying a substitution pattern as in cystobactamids, thereby inactivating the antibiotics.[35] Although the potential clinical relevance of this resistance mechanism is unclear, as *albD* has not been detected in human pathogens yet, we attempted to circumvent it by replacing the amide cleavage site with a 1,2,3-triazole as a bioisoster (Fig. 1).[36] For this purpose, **61** was synthesized in 11 steps and an overall yield of 7% based on a retrosynthetic disconnection in two fragments (ESI Schemes S8 and S9†). The larger fragment **156** was synthesized by coupling 4-ethinylaniline to Fmoc-Asn(Trt)OH, followed by the

Table 4 Antibacterial activity of cystobactamids with modified D rings, given as minimal inhibitory concentrations (MICs) in μg mL^{-1}, and inhibitory activity against DNA gyrase in μM[e]

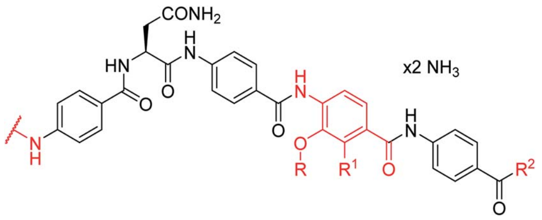

	N-terminus				MIC [μg mL^{-1}]					
Compound	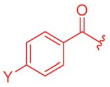 Y	R	R^1	R^2	*E. coli* ΔtolC[a]	*E. coli* WT[b]	*P. ae.* ΔmexAB[a]	*P. ae.* WT[c]	*S. aureus*[d]	*E. coli* gyrase IC$_{50}$ [μM]
Reference 4	**NO$_2$**	**i-Pr**	**OH**	**OH**	**0.125**	**1**	**1**	**>64**	**1**	**0.11**[a]
52	NO$_2$	i-Pr	H	OH	0.06	>64	1	>64	>64	nd
129	NO$_2$	i-Pr	H	OMe	>64	>64	>64	>64	>64	nd
13	NO$_2$	i-Pr	OAllyl	OAllyl	>64	>64	>64	>64	>64	nd
53	NO$_2$	i-Bu	OH	OH	2	>64	>64	>64	1	0.9
54	CN	i-Bu	OH	OH	<0.03	0.25	>64	>64	0.25	nd
55	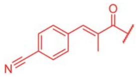	i-Bu	OH	OH	0.06	0.5	>64	>64	0.06	nd

[a] Strain provided by collaborators, see ESI. [b] DSM-1116. [c] PA14. [d] ATCC29213. [e] nd = not determined, *P. ae.* = *P. aeruginosa*.

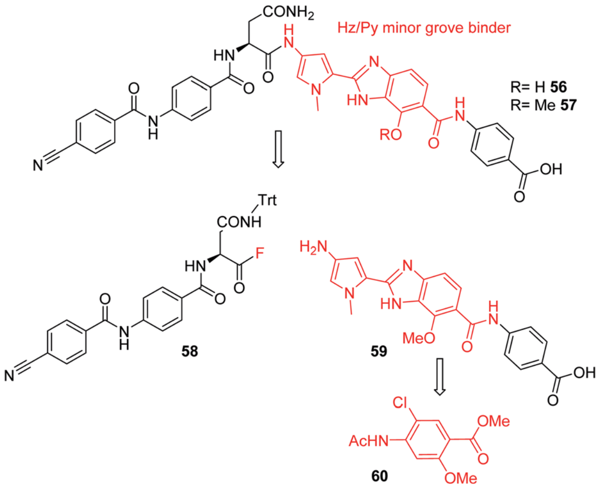

Scheme 5 Retrosynthetic analysis followed for the synthesis of cystobactamid analog **56**. The minor groove binding moiety is highlighted in red.

installation of the diaryl unit **64**. In the synthesis of fragment **154**, the azide moiety was introduced into the advanced intermediate **158** *via* Sandmeyer reaction using *t*Bu-NO and TMS-azide in 70% yield. Finally, fragments **156** and **154** were coupled efficiently *via* copper-catalyzed 1,3-dipolar cycloaddition, and after cleavage of the acid-labile protecting groups, **61** was purified by preparative RP-HPLC. Remarkably, **61** displayed high potency against *E. coli* (MIC = 0.06 μg mL^{-1}) and *S. aureus* (MIC ≤ 0.03 μg mL^{-1}) and a good potency against *P. aeruginosa* (MICs of 2 and 8 μg mL^{-1} against mutant and wild type), in spite of a *ca.* 20-fold weaker inhibition of bacterial gyrase (ESI Table S3†). Thus, the "triazole cystobactamid" **61** has practically the same spectrum coverage as the corresponding analog bearing the original amide **22**, but showed lower inhibitory properties at the molecular target. The stability of **61** was first tested in an *in vitro* assay with recombinant, purified AlbD. While albicidin and **22** were efficiently cleaved into their corresponding tetra- and dipeptides following a 6 h incubation with AlbD, **61** remained fully stable under these conditions (Fig. 1 and ESI Fig. S2–S4†). Further evidence that **61** indeed breaks AlbD-mediated resistance was obtained by MIC data against the AlbD producer *P. dispersa*: whereas *P. dispersa* was resistant against albicidin (MIC > 64 μg mL^{-1}) and showed limited sensitivity towards the best natural cystobactamid **2** (MIC = 16 μg mL^{-1}), **61** potently inhibited its growth with an MIC of 1 μg mL^{-1}.

Thus, a bioisosteric substitution of the amide bond connecting rings C and D is tolerated, and the overall good spectrum coverage of **61** and its resistance-breaking properties make this molecule an interesting scaffold for further investigations.

E-ring modifications

For the investigation of the C-terminal region of the molecule, a retrosynthetic disconnection was chosen that featured a late-stage introduction of the E-ring (Scheme 6). In a first target compound, the E-ring was completely omitted to yield the

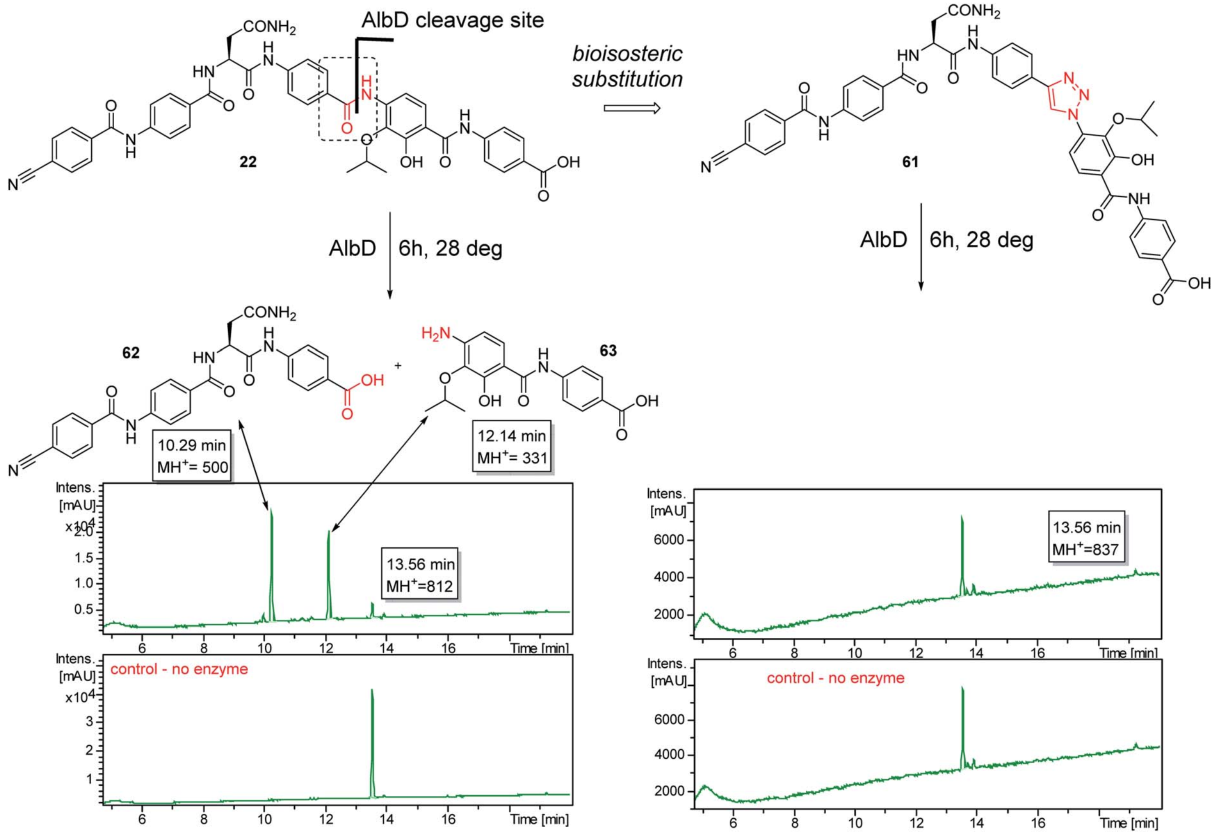

Fig. 1 Design of the AlbD-stable cystobactamid analog **61**, with the amide-triazole replacement highlighted in red. The stabilities of **61** (retention time: 13.56 min) and **22** (retention time: 13.56 min) following a 6 h incubation with AlbD have been monitored by LC/UV/MS. Depicted is the UV absorption (190–400 nm) over time. The degradation products (retention times 10.29 min and 12.14 min) are depicted above the chromatograms.

pentapeptide **67**. This compound was active only against mutant *E. coli* and possessed more than 100-fold reduced enzymatic activity compared to **22** (Table 5). This finding further underlines the importance of the full hexapeptide configuration for the Gram-negative antibacterial activity, that was demonstrated before by the inactive, N-terminally

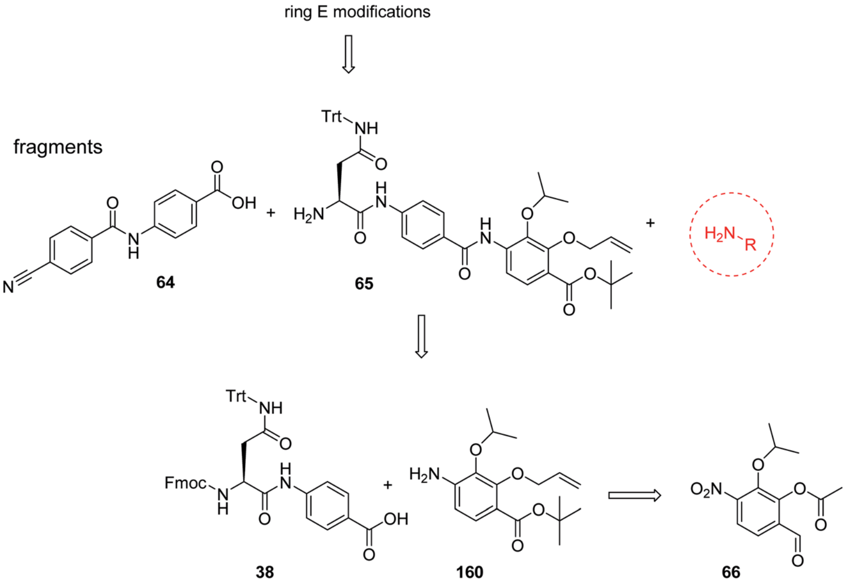

Scheme 6 Retrosynthetic disconnection used for late stage variations of ring E. Fragments **65** and **64** are coupled first, followed by the final installation of ring E.

Table 5 Antibacterial activity of cystobactamids with varying E ring substitution patterns, given as minimal inhibitory concentrations (MICs) in μg mL^{-1}, and inhibitory activity against DNA gyrase in μM[e]

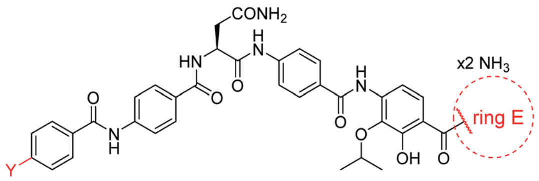

			MIC [μg mL^{-1}]					
Compound	Y	Ring E	*E. coli* ΔtolC[a]	*E. coli* WT[b]	*P. ae.* ΔmexAB[a]	*P. ae.* WT[c]	*S. aureus*[d]	EC gyrase IC$_{50}$ [μM]
Reference 22	**CN**	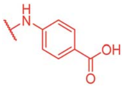	**0.06**	**0.5**	**0.25**	**2**	**0.25**	**0.08**
67	CN	–OH	≤0.03	>64	>64	>64	>64	9.4
68	NO$_2$	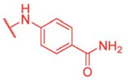	≤0.03	1	>64	>64	64	0.2
69	NO$_2$	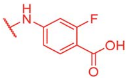	0.125	1	1	>64	2	nd
70	CN	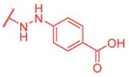	0.25	>64	>64	>64	>64	nd
71	CN	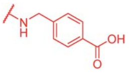	0.25	>64	>64	>64	>64	nd
72	CN	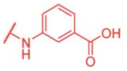	≤0.03	0.5	>64	>64	2	nd
73	CN	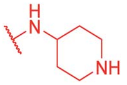	>64	>64	>64	>64	>64	0.5
74	CN	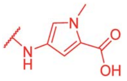	≤0.03	0.5	8	>64	64	nd
75	CN	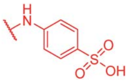	0.25	>64	>64	>64	>64	nd
76	CN	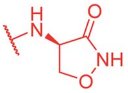	0.5	>64	>64	>64	>64	nd
77	CN	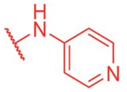	≤0.03	>64	>64	>64	>64	0.9

[a] Strain provided by collaborators, see ESI. [b] DSM-1116. [c] PA14. [d] ATCC29213. [e] nd = not determined, *P. ae.* = *P. aeruginosa*.

truncated albicidin[16] or the tripeptide cystobactamid 507 harboring rings C–E.[37]

Secondly, the C-terminal carboxylic acid of **4** was replaced by an amide in **68**. The compound was highly active in the gyrase assay, but only active against wild type *E. coli*. Introduction of an *ortho*-fluoro atom (**69**) retained the antibacterial spectrum of **4** with no activity against wild type *P. aeruginosa*. Moreover, **129**, the methyl ester analog of **52**, was completely inactive against efflux-impaired and wild type strains (Table 4), and similar effects were observed upon the replacement of the carboxylic acid by a sulfonic acid as in **75**. More drastic modifications of the E-ring were realized by a replacement of the acidic PABA with basic 4-amino-pyridyl (**77**) and 4-amino-piperidyl (**73**) moieties, or the cycloserine **76**. These switches in basicity of the

C-terminus led to a drastic loss of antibacterial activity of these analogs, thereby illustrating the importance of the carboxylic acid. The insertion of a methylene group between the terminal arene and the amide linking it to the D-ring, which disrupts the conjugated π-system, also led to an almost complete loss of activity. It is noteworthy that a similar change between A and B-rings, as in **39**, was not tolerated either (see above).

In contrast, the activity against *E. coli* strains was retained with a *meta*-substituted aminobenzoic acid terminus (as in **72**) and with an *N*-methyl pyrrole moiety (as in **74**) replacing the phenyl ring. However, both analogs clearly lost potency compared to a PABA-C-terminus.

Next, we investigated a conundrum of the E-ring substitution pattern: compared to the first-discovered cystobactamid **3**, both the removal of a substituent (des-isopropoxy, to yield **2**) and the addition of a substituent (hydroxy-919-2 = coralmycin A) were reported to enhance antibacterial activity.[9] To assess whether an unsubstituted or a hydroxy/isopropoxy-substituted E-ring is superior, the latter pattern was combined with the five best N-terminal substitutions reported above (Table 6). The obtained analogs **78–82** showed comparable and high activity against *E. coli* and *S. aureus*, but two of them were less active against *P. aeruginosa* compared to their counterparts **31** and **32**. This led us to conclude that the unsubstituted PABA unit was the superior E ring substitution for a broad spectrum coverage that includes *P. aeruginosa*.

Based on the structural modifications in A, B, D and E rings as well as in selected linker regions described above, a small set of ten cystobactamid derivatives that were most potent on the small microbial strain panel and/or showed activity on the *P. aeruginosa* wild type strain was selected. This set was tested on a larger panel of Gram-negative and -positive pathogens of clinical interest, including *A. baumannii*, *Klebsiella pneumoniae* and other Enterobacteriaceae. The two natural products **1** (synthesized according to the reported experimental procedure),[12] **2** and ciprofloxacin served as reference compounds.

Remarkably, eight derivatives displayed potent (MIC ≤ 1 μg mL^{-1}) activity against *Enterobacter aerogenes*, and three derivatives were active against *K. pneumoniae*, whereas both **1** and **2** were inactive (Table 7). Also spectrum gaps against *E. aerogenes*, *Enterobacter cloacae* and *Proteus mirabilis* could be closed by synthetic analogs.

Table 6 Antibacterial activity of cystobactamids with optimized A-rings and isopropoxy/hydroxyl-substituted E-ring, given as minimal inhibitory concentrations (MICs) in μg mL^{-1}, and inhibitory activity against DNA gyrase in μM[e]

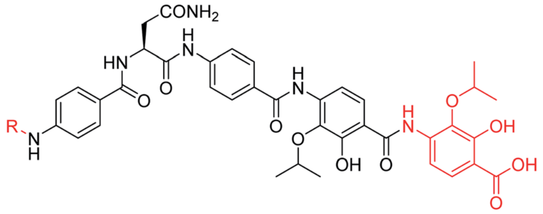

Compound	R	MIC [μg mL^{-1}] *E. coli* ΔtolC[a]	*E. coli* WT[b]	*P. ae.* ΔmexAB[a]	*P. ae.* WT[c]	*S. aureus*[d]	EC gyrase IC$_{50}$ [μM]
Reference 78	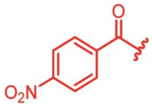	**0.125**	**0.5**	**1**	**>64**	**0.05**	**0.2**
79	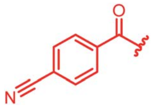	≤0.03	0.25	1	2	≤0.03	0.6
80	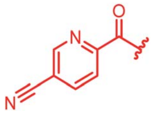	≤0.03	0.06	0.5	>64	≤0.03	nd
81	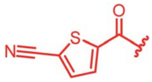	0.06	0.125	2	>64	0.06	nd
82	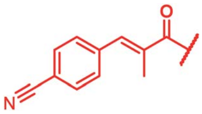	≤0.03	0.125	0.25	1	0.06	0.2

[a] Strain provided by collaborators, see ESI. [b] DSM-1116. [c] PA14. [d] ATCC29213. [e] nd = not determined, *P. ae.* = *P. aeruginosa*.

Table 7 Antibacterial activity of cystobactamids, given as minimal inhibitory concentrations (MICs) in μg mL^{-1} [a]

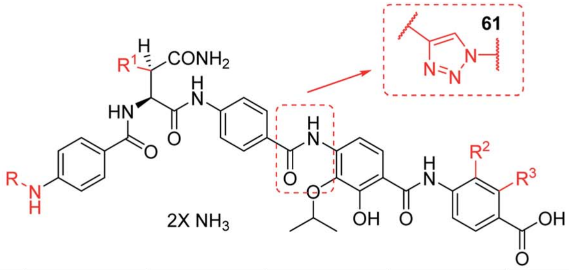

Compounds	22	93	45 (Y=OH)	46 (Y=CN)	31	80	32	81	61
R	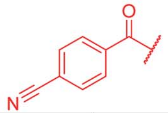		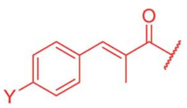		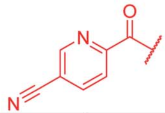		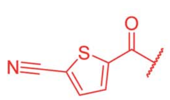		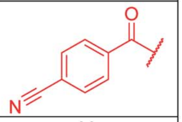
R^1	H	OMe	H		H	H	H	H	H
R^2	H	H	H		H	i-PrO	H	i-PrO	H
R^3	H	H	H		H	OH	H	OH	H

MIC [μg mL^{-1}]	2	Alb	CIP	22	61	45	46	31	32	93	80	81
E. faecalis[1]	1	4	1	0.5	16	0.5	0.5	0.125	0.25	0.125	≤0.03	≤0.03
S. epidermidis[2]	0.5	0.5	0.25	≤0.03	0.125	0.25	≤0.03	1	0.5	≤0.03	≤0.03	≤0.03
S. aureus[3]	0.5	0.5	0.5	0.25	≤0.03	0.25	0.06	≤0.03	0.25	≤0.03	≤0.03	0.06
A. baumannii[4]	1	>64	0.25	1	8	0.25	0.06	0.125	0.125	1	0.25	1
E. coli WT[5]	0.125	0.125	≤0.03	0.5	0.06	0.25	0.125	0.5	0.5	≤0.03	0.06	0.125
E. coli WT-3	0.06	0.06	≤0.03	0.25	16	0.125	0.125	2	1	2	0.5	0.5
E. coli WT-3[6] [*gyrA*(S83L,D87G)]	0.5	0.06	1	0.25	2	0.06	0.125	0.25	0.125	0.25	2	0.5
E. aerogenes[7]	>64	>64	0.125	0.06	1	1	0.25	0.25	0.25	2	1	1
E. cloacae[8]	>64	>64	0.25	0.25	>64	>64	>64	>64	>64	>64	>64	>64
P. aeruginosa WT[9]	2	0.25	0.06	2	8	1	1	≤0.03	≤0.03	0.5	>64	>64
P. aeruginosa ESBL 1[10]	4	16	8	4	16	>64	>64	>64	8	2	>64	>64
P. aeruginosa ESBL 2[11]	2	16	0.25	4	16	2	32	4	8	1	>64	>64
K. pneumoniae[12]	>64	>64	≤0.03	0.5	>64	>64	>64	>64	>64	8	4	1
C. freundii[13]	0.125	≤0.03	≤0.03	≤0.03	0.5	0.125	0.06	≤0.03	≤0.03	≤0.03	0.5	0.5
S. marcescens[14]	>64	>64	0.5	>64	>64	64	>64	>64	>64	>64	>64	>64
P. vulgaris[15]	0.25	≤0.03	≤0.03	0.25	2	0.125	≤0.03	0.06	0.06	0.125	1	1
P. mirabilis[16]	32	>64	0.06	>64	16	2	>64	4	>64	4	8	>64

MIC color scale	≤0.03	0.06	0.125	0.25	0.5	1	2	4	8	16	32	>64

[a] Alb = albicidin, CIP = ciprofloxacin, ESBL = extended spectrum β-lactamases, [1]ATCC-29212, [2]DSM-28765, [3]ATCC29213, [4]DSM-30008, [5]DSM-1116, [6]*E. coli* based on the WT-3 wild type strain, carrying the mutations indicated above, [7]DSM-30053, [8]DSM-30054, [9]PA14 [10]DSM-24600, [11]DSM-46316, [12]DSM-30104, [13]DSM-30039, [14]DSM-30121, [15]DSM-2140, [16]DSM-4479. Additional bacterial strain information is present in the experimental part.

For *A. baumannii*, nine compounds reached MICs ≤ 1 μg mL^{-1}, and the most potent congener **46** had a strongly improved activity (MIC = 0.06 μg mL^{-1}) compared to ciprofloxacin (0.32 μg mL^{-1}) or Cys 861-2 (1 μg mL^{-1}).

The activity against *E. coli* WT-3, a strain that has a *ca.* 100-fold reduced fluoroquinolone sensitivity due to mutations at the active site of gyrase, was also assessed. The fact that the activity of most cystobactamids was not affected by the mutations supports the hypothesis that the binding site of the natural products is different from that of ciprofloxacin.

For all different ring substitutions, compounds that show a reduced gyrase affinity, but still potently kill *E. coli* were observed. This effect may either be due to a particularly high uptake, or due to the presence of a second, yet unidentified antibacterial target. To explore the latter option, a chemoproteomic study using accordingly modified chemical probes is regarded as an attractive future endeavor. To better understand the contributions of uptake to the observed SAR, mass spectrometry-based intracellular concentration measurements in a panel of strains with enhanced outer membrane permeability or impaired efflux are warranted in future studies.

For the cystobactamids **2** and **22** no signs of cytotoxicity, assessed by an MTT (3-(4,5-dimethyl-2-thiazolyl)-2,5-diphenyl-2*H*-tetrazolium bromide)-based assay, were visible within the tested concentration range of 0.1–10 μM. This is in line with previously published cytotoxicity data on cystobactamid analogs.[8,11]

Derivative **93** has the broadest antibacterial spectrum coverage. Remarkably, it possesses activity in the low μg mL^{-1} range against all tested bacteria except of *E. cloacae* and *Serratia marcescens*. These results indicate that the presence of the methoxy-group in the central Asn moiety is beneficial for the spectrum coverage. On the other hand, it is noteworthy that **93** does not exhibit the lowest MIC values against all the tested strains. For example, the lowest MIC values against *K. pneumoniae*, *A. baumannii* and *Enterococcus faecalis* were obtained with **81**/**22**, **46** and **80**/**81**, respectively. This suggests that strain-specific effects influence the activity of cystobactamid derivatives. Given that recent changes in the regulatory guidelines for the clinical testing of antibiotics encourage pathogen-specific antibiotic developments (in addition to classical paths focused on the body site of infection), it is well-conceivable that several different cystobactamids could be developed as narrow-spectrum antibiotics against single pathogens.

The current work allows deriving the following structure–activity relationships (Fig. 2): the full length of the molecule is essential for the activity, shortening it of a single aromatic unit either at the N- or C-terminus led to a complete loss of activity. For optimal inhibition of gyrase and good antibacterial properties, ring A should have a hydrogen bond acceptor, with a cyano group conferring the best antibacterial properties. The optimal position of the substituent on ring A is *para*. The replacement of the phenyl ring with heterocycles is possible and has a beneficial effect on the activity. Finally, the presence of a short rigid spacer, such as a substituted double bond, between ring A and carbonyl is well tolerated. The *para*-connectivity of the aromatic building blocks is also essential for the B-ring, while a relocation of the amino group to the *meta*-position has a drastic negative effect on the activity. The omission of the methoxy group in aliphatic linker region is well tolerated; this finding is in line with a recent study on natural albicidins.[18] However, the enlarged panel of bacterial pathogens investigated in this study suggests that the presence of the methoxy group is overall beneficial for a broader spectrum coverage.

The D-ring represents a critical part of the molecule; the enlargement of the isopropoxy group was associated with a drastic loss of activity; the same is true for a removal or etherification of the hydroxyl group. The latter finding stands in contrast to a recent report on a corresponding dehydroxy-albicidin that retained its activity (against a different panel of strains).[18] Finally, ring E carrying an acidic function was found to be essential for antimicrobial activity. Among all variations tested, the E-ring substitution pattern of the natural product **2** was found to be optimal.

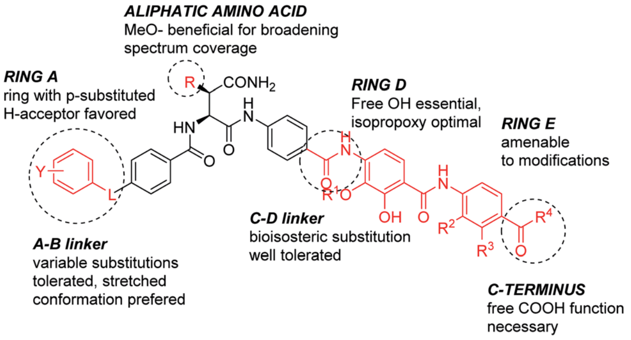
ALIPHATIC AMINO ACID
MeO- beneficial for broadening spectrum coverage
RING A
ring with p-substituted H-acceptor favored
R
CONH$_2$
HN
H N
O
O
Y
L
RING D
Free OH essential, isopropoxy optimal
RING E
amenable to modifications
H N
O
R^{1}O
OH
O
H N
R^2
R^3
R^4
O
A-B linker
variable substitutions tolerated, stretched conformation prefered
C-D linker
bioisosteric substitution well tolerated
C-TERMINUS
free COOH function necessary

Fig. 2 Structure–activity relationships of cystobactamids established in this work.

Cystobactamid-based targeted bacterial imaging

In addition to optimizing the cystobactamid scaffold to an antibiotic, we explored its potential for bacterial imaging. We speculated that structural elements of the cystobactamids could serve as a carrier of imaging moieties due to their capability of penetrating into a broad range of clinically relevant Gram-positive and -negative bacteria. A binding to gyrase is not required to fulfill this purpose.

Indeed, there is a strong medical need to improve the diagnosis of infections at body sites that are hardly accessible for sampling. Therefore, noninvasive molecular probes that can selectively visualize bacteria based on bacteria-specific nutrient uptake pathways,[38,39] enzymatic functions,[40,41] or antibiotic scaffolds[42–44] received considerable attention recently.[45] Based on the structure–relationships established above, the tetrapeptidic N-terminus of **4** was selected as the carrier, and the aromatic rings D and E of the original scaffold were omitted and replaced by an imaging modality (Fig. 3a and b). Ring C was functionalized with an alkynyl moiety to enable a conjugation of the carrier with its payload by click chemistry. For this purpose, the Bodipy-based fluorophore BDP-FL-azide was coupled to the tetrapeptide to yield **85** (Scheme S11†). The free Bodipy–azide **84** was used as non-targeted control. Both **85** and **84** had no effect on bacterial growth (ESI Fig. S6†); however, pronounced differences in their labeling properties were observed: images taken after four hours of incubation clearly indicated a strong fluorescent signal for Gram-positive (*S. aureus*) as well as Gram-negative (*E. coli*, *A. baumannii* and *K. pneumoniae*) bacteria treated with **85**, while that was not the case for free **84** (Fig. 3c, ESI Fig. S9†). This result was confirmed by a quantitative analysis by flow cytometry for *E. coli* (ESI Fig. S7†). Interestingly, an unlabeled subpopulation was observable after treatment with **85**, but the molecular reasons of this phenomenon are unclear at this stage and deserve further attention in future studies.

In additional experiments, the fluorogen-activating-protein/malachite green (FAP/MG) system recently developed by us[38] was applied to probe whether cyctobactamids conjugated with

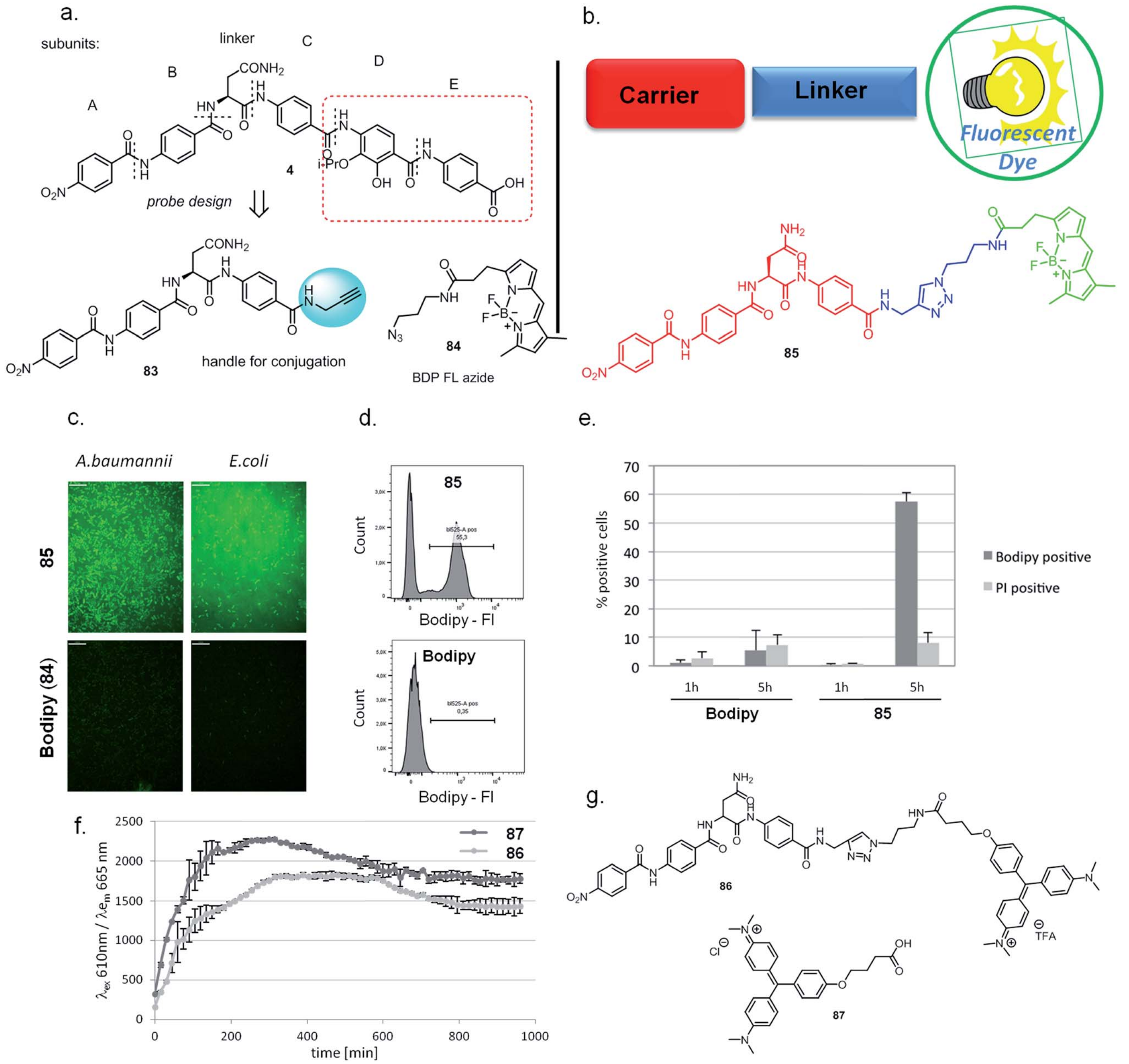

Fig. 3 Labeling of bacterial cells with fluorescent or fluorogenic cystobactamid-conjugate. (a) Design of cystobactamid probe, its structure and the fluorescent dye used. (b) Schematic representation of the basic principle of the strategy and chemical structure of the Bodipy-cystobactamid conjugate. (c) Labeling of indicated bacterial species with Bodipy-conjugate or free Bodipy as monitored by confocal microscopy after 4 h of incubation with 10 μM compound in PBS. Scale bars: 11 μm. (d) Fluorescence intensity (Bodipy-Fl) of free Bodipy or Bodipy-conjugate was quantified by flow cytometry. Histogram depicts Bodipy-Fl *vs.* cell count. Exemplary result of one experiment after 5 h of incubation shown. (e) Bodipy-conjugate uptake quantified by flow cytometry. *E. coli* WT was incubated for 1 or 5 h in PBS with **85** or Bodipy (**84**). Quantification of two replicate experiments of Bodipy-conjugate uptake and propidium iodide (PI) staining as measured by flow cytometry. Plot depicts the percentage of cells classified as Bodipy- or PI-positive. (f) The bacterial uptake of cystobactamid conjugated to the fluorogenic dye malachite green (MG) or free MG was monitored over time with a fluorescence plate reader. **87** (free MG) or **86** (Cysto-MG) were added at a final concentration of 10 μM to *E. coli*_FAP6.2, and the fluorescence was recorded at indicated wavelengths for 16 h. (g) Chemical structures of Cysto-MG conjugate and free MG.

synthetic dyes are internalized by *E. coli*, or whether the compound binds to the outside of the cell wall. For this purpose, the cystobactamid-MG conjugate **86** was synthesized (see the ESI†) and uptake as indicated by fluorescence emission was monitored over time (Fig. 3f and g). The signal reached a maximum after 5 hours and clearly indicated an intracellular accumulation of the cystobactamid-based carrier. The translocation occurred at a rate comparable to that of free MG **87**, which was used as a positive control and presumably enters the cell by passive diffusion.

The findings imply that the C-terminal truncation of cystobactamid leads to the loss of its antibiotic property (in accordance with the SAR findings above), but bacterial recognition and translocation are retained. However, the translocation mechanism of the imaging conjugates might differ from the (hitherto unkown) translocation mechanism of cystobactamid antibiotics. Apart from applications in bacterial imaging, such conjugates may also find use in a Trojan-horse strategy of antibiotic delivery.[6] Future studies, such as competition assays with eukaryotic cells, will clarify whether the N-terminal motif could be utilized to specifically carry payloads into bacterial *vs.* mammalian cells.

In vitro and *in vivo* profile of 22

The cystobactamid analog **22** showed excellent inhibitory properties against Gram-negative and Gram-positive bacteria, while exhibiting low toxicity against HepG2 cells. Stability studies conducted with **2** demonstrated a half-life $t_{1/2}$ of 117 and >400 min in mouse and human hepatocytes, respectively, and stabilities of >90%, 66% and 78% after 4 h incubation in mouse, rat and human plasma, respectively.

The ability of four bacterial strains to develop resistance against **22** was investigated next. We observed frequencies of resistance (FoR) between 3.8×10^{-8} (against *E. coli*) and 1.6×10^{-9} (against *A. baumannii*) at four times MIC, whereas the FoR's of ciprofloxacin were between 2.2×10^{-8} and 1.5×10^{-10} in the same panel. Clones of *A. baumannii* that were resistant to **22** exhibited a fitness loss in terms of impaired growth. However, a fitness loss was not observed for the other strains (ESI Fig. S10†). Serial passaging experiments demonstrated that a high (256 fold) level of resistance against **22** was generated within 4 and 8 passages against *E. coli* ATCC25922ΔtolC and *P. aeruginosa* PA14ΔmexAB. Compared to ciprofloxacin, this level of resistance formation was reached faster in case of *E. coli*, but more slowly in case of *P. aeruginosa* (ESI Fig. S11†). Although an optimal resistance profile (FoR's of $<10^{-9}$ across all strains) is not reached by **22**, the data encouraged us to conduct the first *in vivo* test with a cystobactamid. As the synthesis of **22** was scalable to *a* > 100 mg range, this analog was selected for subsequent studies. First, a dose of 5 mg kg^{-1} of **22** was administered intravenously (i.v.) into male CD-1 outbred mice to determine the pharmacokinetic (PK) parameters of the compound. A half-life around 1 h, an area under the curve (AUC) of around 2 μg mL^{-1} h^{-1} and a volume of distribution of 3.5 L kg^{-1} was observed in plasma (Table S8† and Fig. 4a). Thus, the compound was nearly cleared 8 hours after administration. Next, we determined plasma levels using a subcutaneous route of administration, as this frequently results in an initially slower accumulation and elimination. The maximum concentration $C_{\max}$ after subcutaneous (s.c.) administration of 5 mg kg^{-1} was determined at 128 ng mL^{-1}, and the $t_{\max}$ at 1.7 hours. The mean residence time was augmented from 1 to 3 hours compared to the intravenous route, and the bioavailability was calculated to be 25% (Table S6† and Fig. 4a). A multiple dosing PK study was conducted to assess plasma as well as urine levels after multiple administration of **22**. Initially, **22** was administered at 10 mg kg^{-1} i.v. for a rapid accumulation, then **22** was dosed three times s.c. at 10 mg kg^{-1} after 2, 6 and 10 hours. After 24 hours plasma levels dropped again below 100 ng mL^{-1}. In urine, high compound levels were observed without accumulation. Even after 24 hours urine levels of **22** were higher than 1 μg mL^{-1} (Fig. 4b).

We then performed an *in vivo* tolerance study in male CD-1 mice. Compound **22** was administered four times intravenously (i.v.) every 6 hours in doses of 5, 10 and 20 mg kg^{-1}, corresponding to total doses of 20, 40, and 80 mg kg^{-1} per day, respectively. While no adverse effect was observed at 5 and 10 mg kg^{-1}, one animal in the group treated at 20 mg kg^{-1} showed adverse effects like a moderate loss of activity, appeared ungroomed and pale between the 3rd and 4th dose. These signs remained the same until 24 h. As a result, **22** was administered at maximal single i.v. doses of 12.5 mg kg^{-1} or less to avoid any toxicity issue.

With these encouraging results from PK and tolerance studies, we probed the antibacterial efficacy of **22** in a pharmacodynamics (PD) study using the neutropenic thigh infection model and the *E. coli* strain ATCC25922. Mice were treated with either levofloxacin, **22** (high or low dose) or vehicle (consisting of the same formulation as used for **22**). Treatment of mice started two hours after infection, and bacterial loads in lung, muscle and kidney were assessed 24 hours after infection. In muscle, the bacterial load was reduced by 5 log-units for both **22** dosing groups as well as for the levofloxacin treated group (Fig. 4c). In kidney we observed a complete bacterial clearance in all dosing groups compared to vehicle-treated animals (Fig. 4d). Even lung tissue was reached by **22**, demonstrated by a reduction of the bacterial load by 3 log units (Fig. 4e). Furthermore, we determined the compound levels in muscle, lung and kidney. Whereas we detected around 100 ng mL^{-1} in muscle for both cystobactamid-treated groups (low and high dosing), only low amounts of **22** were observed in kidney and lung tissue, with slightly higher levels for the high dosing group (Table S9†). The experiments show that **22** does not only reach the primary bacterial reservoir in muscle, but is also active in other organs like kidney or lung, which are affected due to secondary seeding of the bacteria.

As no dose dependency was observed in this first *in vivo* experiment, we investigated a lower daily dose in a second trial. In the second *in vivo* experiment, an optimized formulation was used to enable a more conventional dosing scheme with i.v. administrations of **22** at 1, 7, 13, and 19 h post infection in three dose groups (20 mg kg^{-1} per day, 40 mg kg^{-1} per day and 50 mg kg^{-1} per day). The reduction of colony-forming units (cfu) at the lower dose of 20 mg kg^{-1} per day (−3.97 log units) was smaller than those obtained at 40 and 50 mg kg^{-1} per day. In line with the first *in vivo* trial, no dose dependency was observed for the 40 and 50 mg kg^{-1} per day doses (−5.32 and −4.89 log units, respectively). Compared to the cfu count in untreated mice, 1 h post infection, **22** could not only maintain stasis, but reach a reduction of cfu counts at all total doses of 20, 40 and 50 mg kg^{-1} per day (Fig. S12†).

In comparison to fluoroquinolones used as comparators in both *in vivo* experiments, **22** had to be administered more frequently and at higher doses, and the cfu reductions were

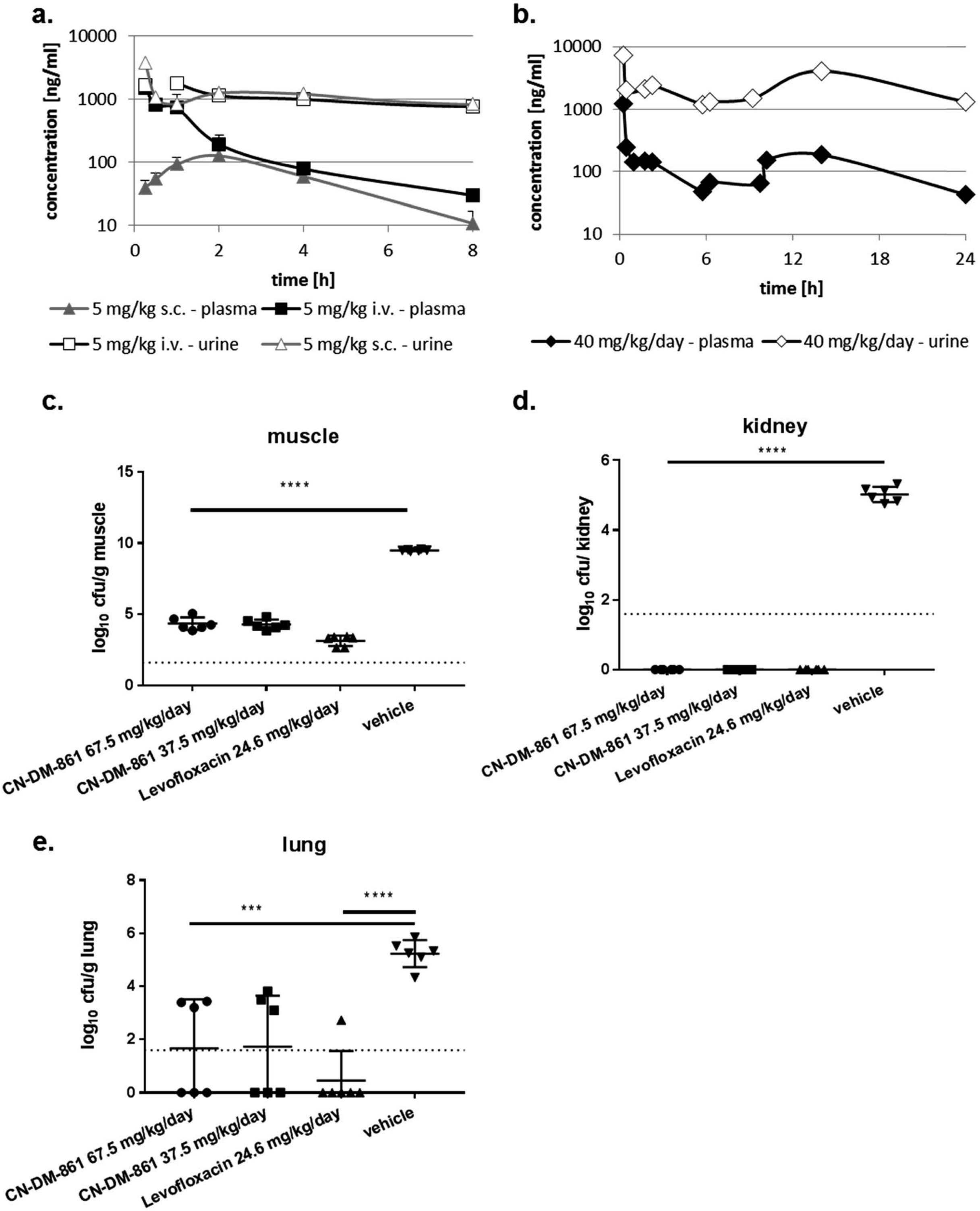

Fig. 4 Pharmacokinetics and pharmacodynamics of **22** (CN-DM-861). (a) Compound levels in plasma and urine after 5 mg kg^{-1} i.v. and s.c. administration into CD-1 mice ($n = 3$). (b) Compound levels in plasma and urine after 10 mg kg^{-1} i.v. at $t = 0$ h and 10 mg kg^{-1} s.c. at $t = 2$, 6 and 10 h into CD-1 mice ($n = 3$). (c–e) Neutropenic thigh infection model in neutropenic CD-1 mice ($n = 6$). The *E. coli* strain ATCC25922 was used that was sensitive to **22** (MIC = 0.02 μg mL^{-1}) and levofloxacin (MIC = 0.04 μg mL^{-1}). Cfu were determined in muscle (c), kidney (d) and lung (e). 8.2 mg kg^{-1} levofloxacin was administered i.p. at $t = 2$, 6 and 10 h and served as a positive control. Vehicle-treated animals received vehicle used for **22** at $t = 2$ h (i.v.) and $t = 4$,8 and 12 h (s.c.). **22** was administered in two dosing groups: group 1 were administered 7.5 mg kg^{-1} i.v. at $t = 2$ h and 20 mg kg^{-1} s.c. at $t = 4$, 8 and 12 h. Group 2 were administered 7.5 mg kg^{-1} i.v. at $t = 2$ h and 10 mg kg^{-1} s.c. at $t = 4$, 8 and 12 h. ***$p < 0.001$; ****$p < 0.0001$.

slightly lower, implying that the *in vivo* efficacy of **22** is slightly inferior to the gold standard in this model.

In summary, the first *in vivo* proof of concept for a cystobactamid (or any other PABA-based antibiotic) strongly encourages the further optimization and development of this novel antibiotic class.

Conclusions

Based on the recently established synthetic access to cystobactamids, we developed three different synthetic routes for a first, extensive SAR study at five different positions of the molecule. The antibacterial activity of cystobactamids was substantially improved and/or tuned against several, medically relevant Gram-negative pathogens. While the overall architecture of the cystobactamids could not be altered, substantial structural modifications (*e.g.* amide replacements, heterocycles) were tolerated or even favorable, illustrating the optimization potential of this antibiotic lead structure. The functional versatility of the scaffold was demonstrated by conjugates that were devoid of an antibiotic activity, but served as bacterial imaging probes. Finally, a first proof of concept *in vivo* was provided in a neutropenic thigh infection model in mice using the optimized cystobactamid analog **22**. Overall, the current study leverages and highlights the great potential of this novel chemical scaffold to yield new antibiotics against resistant bacterial pathogens.

Funding

The study was funded by an internal Pre4D grant of the HZI and by a scholarship of the HZI graduate school for G. Testolin. The studies were co-funded by the German Centre for Infection Research (DZIF; Grant no TTU09.710) and the BMBF Project "Wirkstoffentwicklung auf Basis von Naturstoffen zur Bekämpfung von Infektionskrankheiten" (no GGNATM27).

Authors contribution

GT designed and synthesized cystobactamids, analyzed the data and wrote the manuscript. CG, TM, AB, AR, CL, MMH, WAME designed and synthesized cystobactamids. JvdH, CG and JK performed AlbD-related experiments. VF performed imaging experiments. KC, HP, JK, AV and JH profiled cystobactamids in antibacterial and gyrase and resistance assays. KR and SS performed *in vivo* experiments. RWH, RM, MB designed studies, analyzed data and wrote the manuscript.

Conflicts of interest

GT, MB, CG, RM, JH, HP, MH, WAME, RWH and AR are co-inventors on patent applications on natural and synthetic cystobactamids.

Acknowledgements

The animal studies were conducted in accordance with the recommendations of the European Community (Directive 86/609/EEC, 24 November 1986). All animal procedures for experiments depicted in Fig. 4 were performed in strict accordance with the German regulations of the Society for Laboratory Animal Science (GV-SOLAS) and the European Health Law of the Federation of Laboratory Animal Science Associations (FELASA). Animals were excluded from further analysis if sacrifice was necessary according to the human endpoints established by the ethical board. The experiments were approved by the ethical board of the Niedersächsisches Landesamt für Verbraucherschutz und Lebensmittelsicherheit, Oldenburg, Germany (LAVES; permit No. and 33.19-42502-04-15/1857). We also thank Ulrike Beutling and Heike Overwin for HRMS and LCMS measurements, and Frank Surup and Christel Kakoschke for NMR measurements. We thank Carine Taillier, Nathalie Semenadisse, and Laurence Conraux for resistance studies. The *in vivo* tolerance studies and the animal studies depicted in Fig. S12† were performed in strict accordance under the UK Home office License and the European Health Law of the Federation of Laboratory Animal Science Associations (FELASA). The study was approved by the Agenda Resources (Alderley Park) Animal Welfare and Review Board (Project Licence No. PA67E0BAA E5). We thank Janine Schreiber and Jennifer Wolf for technical assistance.

References

1 M. S. Butler, M. A. Blaskovich and M. A. Cooper, *J. Antibiot.*, 2017, **70**, 3–24.
2 E. Tacconelli, E. Carrara, A. Savoldi, S. Harbarth, M. Mendelson, D. L. Monnet, C. Pulcini, G. Kahlmeter, J. Kluytmans, Y. Carmeli, M. Ouellette, K. Outterson, J. Patel, M. Cavaleri, E. M. Cox, C. R. Houchens, M. L. Grayson, P. Hansen, N. Singh, U. Theuretzbacher and N. Magrini, *Lancet Infect. Dis.*, 2018, **18**, 318–327.
3 L. L. Silver, *Clin. Microbiol. Rev.*, 2011, **24**, 71–109.
4 R. Tommasi, D. G. Brown, G. K. Walkup, J. I. Manchester and A. A. Miller, *Nat. Rev. Drug Discovery*, 2015, **14**, 529–542.
5 M. F. Richter, B. S. Drown, A. P. Riley, A. Garcia, T. Shirai, R. L. Svec and P. J. Hergenrother, *Nature*, 2017, **545**, 299–304.
6 P. Klahn and M. Brönstrup, *Nat. Prod. Rep.*, 2017, **34**, 832–885.
7 B. S. Moore, G. T. Carter and M. Brönstrup, *Nat. Prod. Rep.*, 2017, **34**, 685–686.
8 S. Baumann, J. Herrmann, R. Raju, H. Steinmetz, K. I. Mohr, S. Hüttel, K. Harmrolfs, M. Stadler and R. Müller, *Angew. Chem., Int. Ed.*, 2014, **53**, 14605–14609.
9 Y. J. Kim, H. J. Kim, G. W. Kim, K. Cho, S. Takahashi, H. Koshino and W. G. Kim, *J. Nat. Prod.*, 2016, **79**, 2223–2228.
10 S. Cociancich, A. Pesic, D. Petras, S. Uhlmann, J. Kretz, V. Schubert, L. Vieweg, S. Duplan, M. Marguerettaz, J. Noëll, I. Pieretti, M. Hügelland, S. Kemper, A. Mainz, P. Rott, M. Royer and R. D. Süssmuth, *Nat. Chem. Biol.*, 2015, **11**, 195–197.
11 S. Hüttel, G. Testolin, J. Herrmann, T. Planke, F. Gille, M. Moreno, M. Stadler, M. Brönstrup, A. Kirschning and R. Müller, *Angew. Chem., Int. Ed.*, 2017, **56**, 12760–12764.

12 J. Kretz, D. Kerwat, V. Schubert, S. Grätz, A. Pesic, S. Semsary, S. Cociancich, M. Royer and R. D. Süssmuth, *Angew. Chem., Int. Ed.*, 2015, **54**, 1969–1973.

13 D. Trauner, B. Cheng and R. Müller, *Angew. Chem., Int. Ed.*, 2017, **56**, 12755–12759.

14 T. Planke, M. Moreno, S. Hüttel, J. Fohrer, F. Gille, M. D. Norris, M. Siebke, L. Wang, R. Müller and A. Kirschning, *Org. Lett.*, 2019, **21**, 1359–1363.

15 M. Moeller, M. D. Norris, T. Planke, K. Cirnski, J. Herrmann, R. Müller and A. Kirschning, *Org. Lett.*, 2019, **21**, 8369–8372.

16 D. Kerwat, S. Grätz, J. Kretz, M. Seidel, M. Kunert, J. B. Weston and R. D. Süssmuth, *ChemMedChem*, 2016, **11**, 1899–1903.

17 S. Grätz, D. Kerwat, J. Kretz, L. von Eckardstein, S. Semsary, M. Seidel, M. Kunert, J. B. Weston and R. D. Süssmuth, *ChemMedChem*, 2016, **11**, 1499–1502.

18 L. von Eckardstein, D. Petras, T. Dang, S. Cociancich, S. Sabri, S. Grätz, D. Kerwat, M. Seidel, A. Pesic, P. C. Dorrestein, M. Royer, J. B. Weston and R. D. Süssmuth, *Chem.–Eur. J.*, 2017, **23**, 15316–15321.

19 L. Rostock, R. Driller, S. Grätz, D. Kerwat, L. von Eckardstein, D. Petras, M. Kunert, C. Alings, F. J. Schmitt, T. Friedrich, M. C. Wahl, B. Loll, A. Mainz and R. D. Süssmuth, *Nat. Commun.*, 2018, **9**, 3095.

20 R. O'Shea and H. E. Moser, *J. Med. Chem.*, 2008, **51**, 2871–2878.

21 K. Sakamoto, K. Sato, A. Shigenaga, K. Tsuji, S. Tsuda, H. Hibino, Y. Nishiuchi and A. Otaka, *J. Org. Chem.*, 2012, **77**, 6948–6958.

22 X. Hu, S. J. Dawson, Y. Nagaoka, A. Tanatani and I. Huc, *J. Org. Chem.*, 2016, **81**, 1137–1150.

23 P. Marfey, *Carlsberg Res. Commun.*, 1984, **49**, 591–596.

24 K. Fujii, Y. Ikai, T. Mayumi, H. Oka, M. Suzuki and K.-I. Harada, *Anal. Chem.*, 1997, **69**, 3346–3352.

25 K. Fujii, Y. Ikai, H. Oka, M. Suzuki and K.-I. Harada, *Anal. Chem.*, 1997, **69**, 5146–5151.

26 D. Renneberg and P. B. Dervan, *J. Am. Chem. Soc.*, 2003, **125**, 5707–5716.

27 M. F. Brown, M. J. Mitton-Fry, J. T. Arcari, R. Barham, J. Casavant, B. S. Gerstenberger, S. Han, J. R. Hardink, T. M. Harris, T. Hoang, M. D. Huband, M. S. Lall, M. M. Lemmon, C. Li, J. Lin, S. P. McCurdy, E. McElroy, C. McPherson, E. S. Marr, J. P. Mueller, L. Mullins, A. A. Nikitenko, M. C. Noe, J. Penzien, M. S. Plummer, B. P. Schuff, V. Shanmugasundaram, J. T. Starr, J. Sun, A. Tomaras, J. A. Young and R. P. Zaniewski, *J. Med. Chem.*, 2013, **56**, 5541–5552.

28 C. J. McPherson, L. M. Aschenbrenner, B. M. Lacey, K. C. Fahnoe, M. M. Lemmon, S. M. Finegan, B. Tadakamalla, J. P. O'Donnell, J. P. Mueller and A. P. Tomaras, *Antimicrob. Agents Chemother.*, 2012, **56**, 6334–6342.

29 F. Collin, S. Karkare and A. Maxwell, *Appl. Microbiol. Biotechnol.*, 2011, **92**, 479–497.

30 J. W. Trauger, E. E. Baird and P. B. Dervan, *Chem. Biol.*, 1996, **3**, 369–377.

31 P. B. Dervan and B. S. Edelson, *Curr. Opin. Struct. Biol.*, 2003, **13**, 284–299.

32 C. Kaduk, H. Wenschuh, M. Beyermann, K. Forner, L. A. Carpino and M. Bienert, *Lett. Pept. Sci.*, 1996, **2**, 285–288.

33 L. A. Carpino, M. Beyermann, H. Wenschuh and M. Bienert, *Acc. Chem. Res.*, 1996, **29**, 268–274.

34 L. A. Carpino, D. Sadat-Aalaee, H. G. Chao and R. H. DeSelms, *J. Am. Chem. Soc.*, 1990, **112**, 9651–9652.

35 L. Vieweg, J. Kretz, A. Pesic, D. Kerwat, S. Grätz, M. Royer, S. Cociancich, A. Mainz and R. D. Süssmuth, *J. Am. Chem. Soc.*, 2015, **137**, 7608–7611.

36 E. Bonandi, M. S. Christodoulou, G. Fumagalli, D. Perdicchia, G. Rastelli and D. Passarella, *Drug Discovery Today*, 2017, **22**, 1572–1581.

37 M. Moreno, W. A. M. Elgaher, J. Herrmann, N. Schläger, M. M. Hamed, S. Baumann, R. Müller, R. W. Hartmann and A. Kirschning, *Synlett*, 2015, **26**, 1175–1178.

38 K. Ferreira, H. Y. Hu, V. Fetz, H. Prochnow, B. Rais, P. P. Müller and M. Brönstrup, *Angew. Chem., Int. Ed.*, 2017, **56**, 8272–8276.

39 X. Ning, S. Lee, Z. Wang, D. Kim, B. Stubblefield, E. Gilbert and N. Murthy, *Nat. Mater.*, 2011, **10**, 602–607.

40 Y. Kong, H. Yao, H. Ren, S. Subbian, S. L. Cirillo, J. C. Sacchettini, J. Rao and J. D. Cirillo, *Proc. Natl. Acad. Sci. U. S. A.*, 2010, **107**, 12239–12244.

41 F. J. Hernandez, L. Huang, M. E. Olson, K. M. Powers, L. I. Hernandez, D. K. Meyerholz, D. R. Thedens, M. A. Behlke, A. R. Horswill and J. O. McNamara, *Nat. Med.*, 2014, **20**, 301–306.

42 M. van Oosten, T. Schäfer, J. A. Gazendam, K. Ohlsen, E. Tsompanidou, M. C. de Goffau, H. J. Harmsen, L. M. Crane, E. Lim, K. P. Francis, L. Cheung, M. Olive, V. Ntziachristos, J. M. van Dijl and G. M. van Dam, *Nat. Commun.*, 2013, **4**, 2584.

43 Q. Zhang, Q. Wang, S. Xu, L. Zuo, X. You and H. Y. Hu, *Chem. Commun.*, 2017, **53**, 1366–1369.

44 L. Zhang, Y. Liu, Q. Zhang, T. Li, M. Yang, Q. Yao, X. Xie and H. Y. Hu, *Anal. Chem.*, 2018, **90**, 1934–1940.

45 X. Wang and N. Murthy, *Sci. Transl. Med.*, 2014, **6**, 259fs243.